World Academy of Science, Engineering and Technology
International Journal of Aerospace and Mechanical Engineering
Vol:10, No:10, 2016

Numerical Simulation of Plasma Actuator Using OpenFOAM

H. Yazdani, K. Ghorbanian

***Abstract*—**This paper deals with modeling and simulation of the plasma actuator with OpenFOAM. Plasma actuator is one of the newest devices in flow control techniques which can delay separation by inducing external momentum to the boundary layer of the flow. The effects of the plasma actuators on the external flow are incorporated into Navier-Stokes computations as a body force vector which is obtained as a product of the net charge density and the electric field. In order to compute this body force vector, the model solves two equations: One for the electric field due to the applied AC voltage at the electrodes and the other for the charge density representing the ionized air. The simulation result is compared to the experimental and typical values which confirms the validity of the modeling.

***Keywords*—**Active flow control, flow field, OpenFOAM, plasma actuator.

I. Introduction

PRODUCTION of plasma using a variety of methods such as electrical discharge spark, DC, AC and RF is possible [1]. The particular shape of the dielectric barrier discharge plasma aerodynamic actuator which in recent years has been of interest to researchers and industrialists. Dielectric-barrier discharges are very attractive for industrial applications because they can provide non-equilibrium plasma conditions at about atmospheric pressure.

The single dielectric barrier aerodynamic plasma actuator is a dielectric barrier discharge plasma in which an asymmetric arrangement of electrodes (one exposed, one encapsulated) leads to momentum coupling into natural air. It has shown substantial promise as an aerodynamic flow control device combining the desirable attributes of high control authority, electrical efficiency, and simplicity of construction (no moving parts). A schematic representation of a typical single asymmetric DBD plasma actuator is depicted in Fig. 1 [2], [3]. The actuator consists of two electrodes that are separated by a thin dielectric material such as Teflon, Kapton and etc.

Among the active flow control techniques, the plasma actuator has been demonstrated to be effective in several applications such as flow separation. In the last few years a lot of research on plasma actuator as a mechanism to flow control flow has been done [4]. One of the major areas for applications of plasma actuator is the gas turbine which has the potential to lead to significant benefits in improved efficiency [5]. Although this method has been beneficial in laboratory tests, the incorporation of such systems into actual applications in not straightforward. In fact, an experimental approach requires numerous costly and time consuming iterations. In other word, computational fluid dynamics (CFD) offers an alternative method for understanding complicated flow field and plasma actuator impacts.

Hamidreza Yazdani, PhD candidate, and Dr. Kaveh Ghorbanian are with the Department of Aerospace Engineering at Sharif University of Technology, Tehran, Iran (e-mail: hra.yazdani@gmail.com, Ghorbanian@sharif.edu).

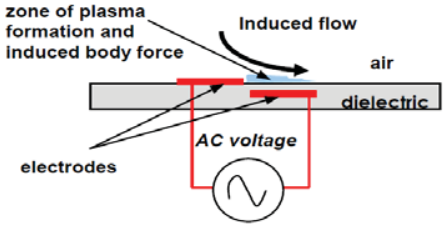

Fig. 1 Plasma actuator [8]

When a high-voltage AC is applied to the electrodes causes the air in their vicinity to weakly ionized. This process, during which some light is emitted by the plasma, is also known as glow discharge or dielectric barrier discharge. The basis of the actuators is the generation of a body force vector that results from the combination of the local ionization of the air over the actuator, and the electric field produced by the geometric design of electrodes and dielectric layer [6]. An induced body force on the rest of the air in this region is the outcome that creates an attenuated jet adjacent to the surface [7]-[8].

II. Flow Control

The modeling of the plasma actuator's effects on the flow is a very active area of research. In recent years, has been widely studied on plasma actuator as flow control. Plasma actuator with electrodes that are asymmetrical, first time was introduced by Roth and colleagues as flow control system in 1990 as boundary layer control by [9]. In fact, the effectiveness of plasma actuators in controlling flow separation has been demonstrated by several researchers. Examples of various applications include, wing section leading edge separation control by [10], unsteady vortex generation by [11], separation control on low pressure turbine blades by [12], tip clearance control in turbines [13] and delay of rotating stall in compressors by [14]-[16]. The outcomes from these experiments demonstrate that various parameters must be taken into account for flow control effectively. Actuators' position on the surface, orientation, electrodes size, relative position of embedded and exposed electrodes, applied voltage, and frequency are these important parameters.

III. Plasma Modeling and Computations

A. Modeling

How to model the effects of plasma actuator on the flow is still a challenge. So far, different models to simulate its impact has been raised around it. These models can be divided in two main categories [17]: (1) The scientific models aimed at reproducing as exactly as possible the microscopic phenomenon taking place during the ionization process and (2) The "engineering" models or phenomenological models aimed at reproducing the global or macroscopic effects of plasma actuators on the flow. Many models have recently been developed to simulate the fluid dynamic effect of plasma actuators for flow control. Shyy et al. [18] proposed a more sophisticated, yet simple, model that provided a time-averaged linear two-dimensional body force distribution in terms of the actuator size and input voltage amplitude and frequency. Suzen et al. [19] proposed a model that is intended to produce a more realistic charge density and body force distribution based on actuator geometry and the nature of the fluid and dielectric material. The amplitude of this body force field could then be modulated in time with the alternating voltage input. Orlov et al. [12] used a network of electrical elements to model the glow discharge region over the encapsulated electrode to obtain a more accurate spatial and time variation of the induced body force.

Among the plasma actuators models of average complexity capable of producing a body force distribution [14], the one by [19] gives the spatial body force distribution that generally resembles those simulated with the most sophisticated models. This model is thus used to obtain the representative time-averaged spatial body force distribution. The associated equations for the electrical potential and charge distributions were discretized in cell-centered form in cylindrical coordinates.

The most recent ones model the actuator as a spatial body force distribution. Among the simplest of these models, that of Shyy et al. [18] propose a time-averaged (over an AC cycle) linear spatial body force distribution based on the size of the electrodes, the actuator's input voltage/frequency and a few properties of air. Suzen et al. [19] developed a more sophisticated model solving the spatial distribution of electric potential and charge density around the actuator as a function of actuator's input voltage magnitude and geometry (electrode length and thickness) and dielectric material properties to obtain a more realistic force distribution. The instantaneous amplitude of the body force vectors is then scaled by the AC voltage input shape to get the variation of the force distribution over time. Orlov et al. [12] developed a higher fidelity plasma generation model which more accurately reproduce the time variation of the body force during the AC cycle through the capture of the time variation of the plasma generation. To do this, they divided the region over the dielectric surface into a network of electric circuits to allow the computation of the electric potential distribution along the dielectric surface over the covered electrode at each time step during the AC cycle. As the level of complexity in the models increases, more and more plasma features are taken into account. However, it is important to mention that no model (even the more sophisticated one) can pretend to be able to generate the exact body force distribution corresponding to specific actuator's geometry and input voltage.

B. Computations

The plasma actuators consist of two electrodes separated by a dielectric layer. The actuator is placed in the surface with one electrode exposed to the surroundings and the other one embedded in the surface below the dielectric layer (Fig. 1) [19]. When a high AC voltage is applied to the electrodes, a purplish glow plasma is created. In fact, this shape will cause the air in their vicinity to weakly ionize. The ionized air in the presence of the electric field gradient caused by the electrodes, leads to a body force vector acting on the external flow. This body force can be expressed in terms of the applied voltage and incorporated into the Navier-Stokes equations. By neglecting magnetic forces, the electro-hydrodynamic (EHD) force can be expressed as

$$\overrightarrow{f_B} = \rho_c \vec{E} \tag{1}$$

where, $\overrightarrow{f_B}$ is the body force per unit volume, ρ_c is net the charge density and E is the electric field. Due to the time variation of the magnetic field in the case of plasma is negligible the Maxwell's equations give rise to

$$\nabla \times \mathrm{E} \approx 0 \tag{2}$$

Therefore, electric field can be derived from the gradient of a scalar potential [20]-[21].

$$\vec{\mathrm{E}} = -\nabla\Phi \tag{3}$$

Gauss's law yields:

$$\nabla.\left(\varepsilon\vec{E}\right) = \rho_c \tag{4}$$

where ε is the permittivity that is the resistance of the material when placed in an electric field. The permittivity can be expressed as:

$$\varepsilon = \varepsilon_r \varepsilon_0 \tag{5}$$

where ε_r is the relative permittivity of the medium, and ε_0 is the permittivity of free space. In fact, calculations show that the effect of changes in temperature and viscosity on the body force can be neglected and Plasma region to be assumed to be more like a source. Since the gas particles are weakly ionized, we can assume the potential Φ can be decoupled into two parts: one being a potential due to the external electric field, ϕ, and the other being a potential due to the net charge density in the plasma, φ,

$$\Phi = \phi + \varphi \tag{6}$$

If we presume that Debye thickness is small and the amount of charge on the wall is not large, the distribution of charged particles in the domain is a function of potential on the wall because the electric charge is affected a little by the external electric field. Hence, we can compose two separate equations in terms of these two possibilities, one for the external electric field because of the applied voltage at the electrodes [19]

$$\nabla.(\varepsilon_r \nabla \emptyset) = 0 \tag{7}$$

and another one for the potential due to the charged particles:

$$\nabla.(\varepsilon_r \nabla \varphi) = -({}^{\rho_c}/_{\varepsilon_0}) \tag{8}$$

Equation (7) is solved for the electric potential, ϕ, using the applied voltage on the electrodes as boundary conditions. The boundary conditions and the computational domain for Equation (7) are shown in Fig. 2. Equation (7) is solved with the appropriate ε_r value on both the air side and the wall and boundary condition. For air, $\varepsilon_r = 1$ .We chose Kapton as the dielectric material, as in the experiments and it has a ε_r value of 2.7.

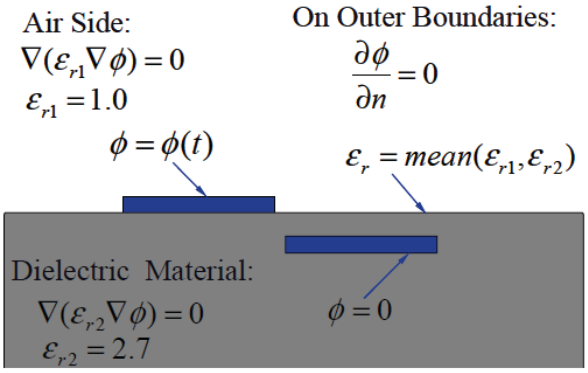

Fig. 2 Computational domain and boundary conditions for (7)

On the wall-air interface harmonic mean of ε_{r1} and ε_{r2} must be used in order to conserve electric field as shown in Fig. 3. (Because the electric field is simulated with better accuracy.) In Fig. 3, point 1 is on air side and point 2 is in the dielectric material, with point *f* on the interface.

At the dielectric wall and air interface, the electric field is conserved as shown in Fig. 3 by writing:

$$-\varepsilon_f\left[\frac{\partial\emptyset}{\partial x}\right]_f = -\varepsilon_1\left[\frac{\partial\emptyset}{\partial x}\right]_{1\to f} = -\varepsilon_2\left[\frac{\partial\emptyset}{\partial x}\right]_{f\to 2} \tag{9}$$

By using the electric analogy as shown in Fig. 3, the interfacial permittivity, ε_f , should take the harmonic mean of the permittivity of air, ε_1 , and the permittivity of dielectric material, ε_2 : (Using interpolation between measurement unit 1 and unit electricity dielectric material 2, 3 can be calculated)

$$\varepsilon_f = \frac{\varepsilon_1\varepsilon_2}{\varepsilon_1\frac{\Delta x_{f2}}{\Delta x_{12}}+\varepsilon_2\frac{\Delta x_{1f}}{\Delta x_{12}}} \tag{10}$$

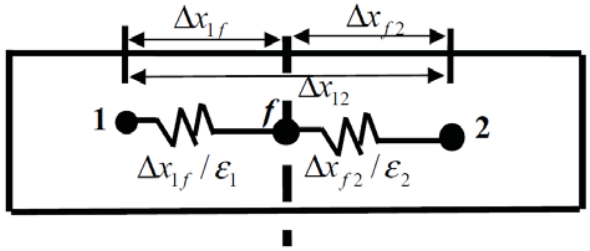

Fig. 3 The interfacial permittivity

Applied AC voltage imposed at the exposed (upper) electrode as boundary condition is:

$$\emptyset(t) = \emptyset^{max} f(t) \tag{11}$$

The wave form function, $f(t)$, can be a sine wave given by:

$$f(t) = \sin(2\pi wt) \tag{12}$$

Or it can be a square wave given by:

$$f(t) = 1 \ for \ \sin(2\pi\omega t) \geq 0$$
$$f(t) = -1 \ for \ \sin(2\pi\omega t) < 0 \tag{13}$$

where ω is the frequency and $\emptyset^{max}$ is the amplitude. The embedded electrode is prescribed as ground by setting the electric potential to zero on that electrode. At the outer boundaries, $\frac{\partial\emptyset}{\partial n} = 0$ is assumed. Next, we consider the electric potential due to the net charge in the plasma, (8). The net charge density within the plasma at any point is24:

$$\rho_c/\varepsilon_0 = \frac{e(n_i-n_e)}{\varepsilon_0} \approx -\frac{en_0}{\varepsilon_0}\left[\exp\left(\frac{e\varphi/KT_i)+\exp(e\varphi}{KT_e}\right)\right] \tag{14}$$

where, e is elementary charge; n_i and n_e are the ion and electron densities in the plasma; n_e is the background plasma density; k is the Boltzmann's constant; T is the temperature of the species; and φ is the local electric potential. Expanding the exponential functions in a Taylor series for $\varphi << T$, (14) becomes, to lowest order of φ/T;

$$\rho_c/\varepsilon_0 = -(\tfrac{e^2 n_0}{\varepsilon_0})[(1/KT_i) + (1/KT_e)]\varphi \tag{15}$$

Based on the Debye length, λ_d ,

$$(1/\lambda_d^2) = (e^2 n_0/\varepsilon_0)[(1/KT_i) + (1/KT_e)] \tag{16}$$

Equation (15) becomes;

$$\rho_c/\varepsilon_0 = -(1/\lambda_d^2)\varphi \tag{17}$$

The electric potential is:

$$\varphi = -(\lambda_d^2 \rho_c/\varepsilon_0) \tag{18}$$

Substituting (18) in (8) we obtain an equation in terms of the net charge density at any point within the plasma.

$$\nabla.(\varepsilon_r \nabla \rho_c) = \rho_c / \lambda_d^2 \quad (19)$$

Equation (19) is solved for the net charge density, ρ_c , only on the air side of the domain using the boundary conditions shown in Fig. 4.

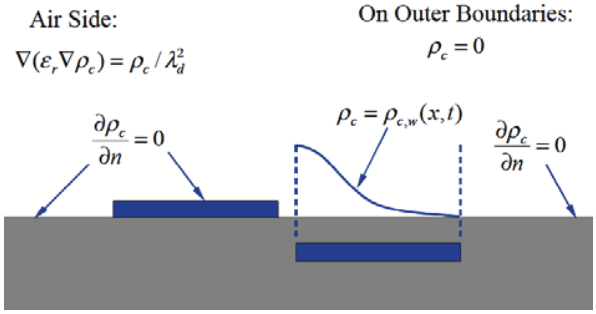

Fig. 4 Computational domain and boundary conditions for (19)

A zero normal gradient for the net charge density is forced on the solid walls aside from the region covering the lower electrode and the charge density is set to zero on the outer boundaries. Therefore, for the net charge density boundary condition applied on the wall above the encapsulated electrode is given by:

$$\rho_{c,w}(x,t) = \rho_c^{max} G(x) f(t) \quad (20)$$

where ρ_c^{max} is the maximum value of the charge density allowed in the domain (in Coulomb/m3), a parameter to be determined later. The variation of the charge density on the wall $\rho_{c,w}$ in the streamwise direction, *x*, is described by a function *G(x)* which can be chosen to resemble the plasma distribution over the embedded electrode. Experimental results [21]-[23]:

$$G(x) = exp[-(x-\mu)^2/2\sigma^2] \quad for\ x \geq 0 \quad (21)$$

In order to solve (7) and (19), the Debye length, (λ_d), maximum charge density on the wall, ρ_c^{max}, scale parameter for charge density distribution, σ , have to be prescribed. These parameters can be calibrated based on a simple experiment having a pure plasma-driven flow in a quiescent environment, as will be explained in the next section. In the computations we have chosen the location parameter μ such that the peak corresponds to the left edge of the embedded electrode as shown in Fig. 4. Moreover, we have assumed that σ takes a value of 0.3 to allow a gradual decay of the charge density distribution from the left edge to the right edge. The values of the frequency and amplitude of the applied voltage, ω and $\emptyset^{max}$ in (12), (13a) and (13b) are given from the experiments.

Once $\emptyset$ and ρ_c are obtained from solutions of (7) and (19) respectively, the resulting body force vector is computed from (1), that is:

$$\overrightarrow{f_b} = \rho_c \vec{E} = \rho_c(-\nabla \emptyset) \quad (22)$$

IV. Results and Discussion

In this study the answer to the above equations around the operator is calculated by coding. Then for the first time volume force is obtained with the help of "OpenFoam" software.

First, to ensure the plasma actuator simulation, flow patterns obtained (Fig. 5) was compared with the results of Suzen's model (Fig. 6) with the conditions shown in Fig. 7, which proved high accuracy in comparison to the model.

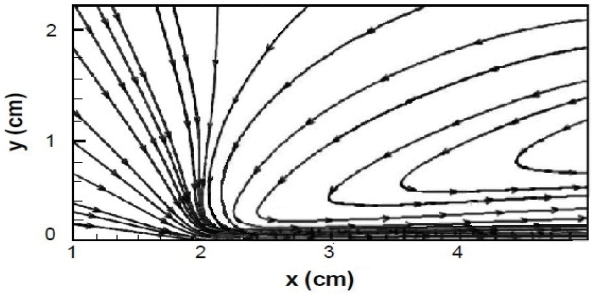

Fig. 5 Streamlines for the plasma actuator in quiescent flow

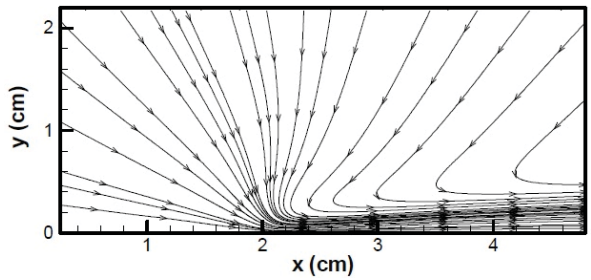

Fig. 6 The results of Suzen [19]

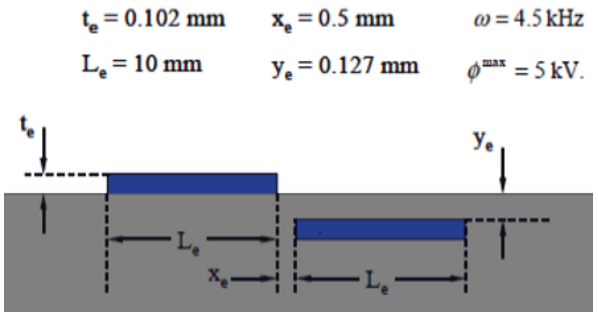

Fig. 7 Experimental set up [22]

From Fig. 5, it is observed that the flow is drawn into the surface region above the embedded electrode by the plasma induced body force. By solving the equations in the OpenFoam software results include: As can be seen in Fig. 8, by applying a magnetic field between two electrodes, the fluctuations in the fluid due to changes in the parameters characteristic of the fluid is appeared.

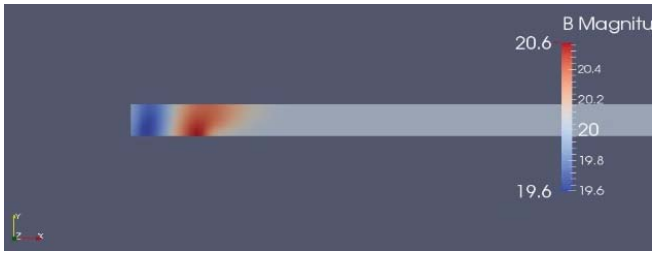

Fig. 8 Magnetic fields

Most of the varying component of magnetic field in the area where the electrodes are closest is seen. In this area, the highest and lowest component of magnetic field occurs while in further areas due to reduced effects of induced field, changes and fluctuations will not be observed. Changes of fluid pressure shown in Fig. 9.

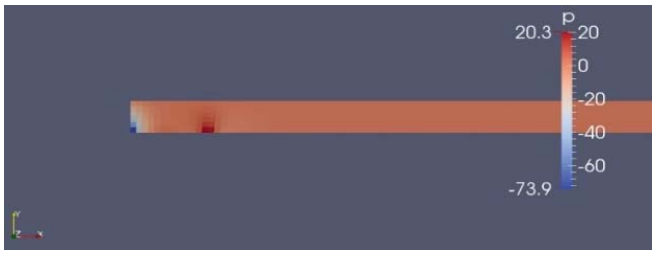

Fig. 9 Pressure changes

It is obvious that the magnetic field between two electrodes effects on the characteristic parameters of flow and causes fluctuations are occurred in the field and causes changes in characteristic parameters of flow be intensified. As can be seen due to the applied voltage and magnetic field between the electrodes, in the area where the electrodes are closest distance will be faced with severe pressure drop. In fact, this pressure drop can be due to start of the fluid flow

The magnetic field causes violation of the law of conservation of mass, which is also why there is a pressure drop. In fact, a fluid that is driven by the magnetic field lines due to ongoing field lines and deploy it to the other electrode mass will not be replaced and pressure drop occurs. Of course pressure drop in normal systems is not too noticeable but this amount will be significant in this very small dimensions. Fig. 10 shows the presence of vortices more accurately.

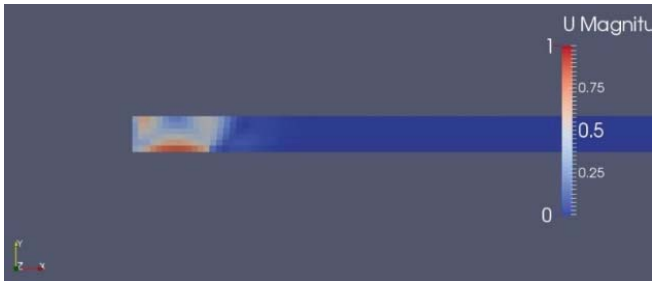

Fig. 10 Vortices speed changes

V. Conclusion

Plasma actuator was simulated for the first time in OpenFOAM software and was validated by comparing with Suzen's model that shows a high-precision modeling has been done. Then, the effects of this actuator on the flow field are presented. This model can be used for active control by using the OpenFOAM software.

References

[1] U. Kogelschatz, B. Eliasson, W. Egli, "From ozone generators to flat television screens: history and future potential of dielectric-barrier discharges," Pure and Applied Chemistry, pp.1819-1828, 1999.
[2] T.C. Corke, C.E. Enloe, and S.P. Wilkinson, "Dielectric Barrier Discharge Plasma Actuators for Flow Control," Annual Review of Fluid Mechanics, 2009.
[3] B. Jayaraman B., Y.C. Cho, and W. Shyy, "Modeling of dielectric barrier discharge plasma actuator," Journal Appl. Phys. 2008.
[4] W.K. Lord, D.G. MacMartin, and T.G. Tillman, "Flow Control Opportunities in Gas Turbine engines," AIAA 2000-2234, 2000.
[5] R. Rivir, R. Sondergaard, J.P. Bons, and J.P. Lake, "Passive and Active control of separation in Gas Turbines," AIAA 200-2235, 2000.
[6] T.C. Corke, M.L. Post, and D.M. Orlov, "Single Dielectric Barrier Discharge Plasma Enhanced Aerodynamics: Physics, Modeling and Applications," Review Article: Experiments in Fluids, v. 46, n. 1, pp.1-26, 2008.
[7] B. Jayarama, Y. Cho, W. Shyy, "Modeling of Dielectric Barrier Discharge Plasma Actuator," 38th AIAA Plasma Dynamics and Lasers Conferences, 2007.
[8] T.C. Corke, M. Post, "Overview of Plasma Flow Control: Concepts, Optimization and Applications," AIAA paper, 2005.
[9] J.R. Roth, D.M. Sherman, and S.P. Wilkinson, "Boundary Layer Flow Control with A one Atmosphere Uniform Glow Discharge Plasma," 36th AIAA Aerospace Sciences Meeting and Exhibits, Reno, 1998.
[10] M.L. Post, T. Corke, "Separation Control on High Angle of Attack Airfoil Using Plasma Actuators," 2003-1024, 2003.
[11] D. Orlov, T. Corke, M. Post, "DNS Modeling of Plasma Array Flow Actuators," Bulletin of the American Physical Society Fluid Dynamics Division, Annual Meeting, 2002.
[12] J. Huang, T.C. Corke, and F.O. Thomas, "Plasma Actuators for Separation Control of Low Pressure Turbine Blades," AIAA- 2003-1027, AIAA 41st Aerospace Sciences Meeting and Exhibit, Reno, NV, January 2003.
[13] S.C. Morris, T.C. Corke, D. Van Ness, J. Stephens, and T. Douville, "Tip Clearance Control Using Plasma Actuators," AIAA- 2005-0782, January 2005.
[14] H.D. Vo, "Control of short length-scale rotating stall inception on A high-speed axial compressor with plasma actuator," ASME Turbo Expo 2008, GT2008-50967, 2008.
[15] H.D. Vo, J.D. Cameron, and S.C. Morris, "Control of short length-scale rotating stall inception on a high-speed axial compressor with plasma actuation," ASME Turbo Expo 2008, GT2008-50967, 2008.
[16] F. Afshari, M. Michaud, and H.D. Vo, "Delay of Rotating Stall in Compressors using Plasma Actuator," International Gas Turbine Institute, 2015.
[17] S. Lemire, H.D. Vo, and M.W. Banner, "Performance Improvement of Axial Compressors and Fans with Plasma Actuation," International Journal of Rotary Machinery, 2009.
[18] W. Shyy, B. Jayarman, and A. Anderson, "Modeling of Glow Discharge-Induced Fluid Dynamics," Journal of Applied Physics, v.92, n.11, PP. 6434-6443.
[19] Y.B. Suzen, P.G. Huang, J.D. Jacob, and D.E. Ashpis, "Numerical Simulations of Plasma Based Flow Control Applications," AIAA Paper 2005.
[20] J.R. Roth, D.M. Sherman, and S.R. Wilkinson, "Electrohydrodynamic Flow Control with a Glow-Discharge Surface Plasma," AIAA Journal, v.38, n.7, 2000.
[21] C.L. Enloe, T.E. McLaughlin, R.D. Van Dyken, K.D. Kachner, E.J. Jamper, T.C. Corke, M. Post, and O. Haddad, "Mechanism and Response of a single Dielectric Barrier Plasma Actuator: Geometric Effects," AIAA Journal, v.42, n.3, 2004.

[22] J.D. Jacob, K. Ramakumar, R. Anthony, and R.B. Rivir,"Control of Laminar and Turbulent Shear Flows Using Plasma Actuators," Fourth International Symposium on Turbulence and Shear Flow Phenomena, TSFP-4, Williamsburg, VA, June 2005.
[23] C.L. Enloe, T.E. McLaughlin, G.I. Font, J.W. Baughn, "Parameterization of Temporal Structure in a Single Dielectric Barrier Aerodynamic Plasma Actuator," AIAA Journal, v.44, n.6, 2006.